Optimal control of femtosecond laser–cluster interactions

T. Martchenko, Ch. Siedschlag, S. Zamith,* H. G. Muller, and M. J. J. Vrakking
FOM Institute for Atomic and Molecular Physics (AMOLF), Kruislaan 407, 1098 SJ Amsterdam, The Netherlands
(Received 6 June 2005; published 3 November 2005)

We present calculations showing that ionization of Xe_N ($N=108-1524$) clusters by intense femtosecond lasers is governed by two mechanisms that have their origin in molecular and plasma physics, respectively. Optimal-control calculations show that a three-pulse sequence optimizes cluster ionization and involves both enhanced ionization and resonant driving of collective electron oscillations. As a result we can understand how ionization in intense laser fields evolves from small molecules to large clusters.

DOI: 10.1103/PhysRevA.72.053202 PACS number(s): 36.40.Gk, 31.15.Qg, 52.50.Jm

I. INTRODUCTION

The interaction of clusters with intense laser fields has become a rapidly developing area of research over the past few years. The physical phenomena resulting from this interaction are determined by the unique properties of clusters, being a bridge system between solids and gas. On the one hand, the high local density of clusters allows strong energy absorption from the irradiating laser field. On the other hand, unlike solids, there is no relaxation of the deposited heat into the bulk due to the small (nanometer-scale) size of clusters. Thus almost 100% of the laser energy can be coupled into a dense cluster jet [1]. The high efficiency of energy absorption leads to cluster explosion and the production of highly charged and energetic ions [2], electrons with keV energies [3,4] and soft-x-ray emission [5] with suitable wavelengths for applications in extreme-ultraviolet (EUV) lithography and microscopy [6].

In order to understand the fundamental physical processes that take place during the laser-cluster interaction and to find a way to maximize the yield of products of the cluster explosion in view of possible applications, it is important to ascertain the optimal conditions for energy coupling from the laser field into the cluster. A number of experimental observations have shown possible ways to increase the laser-cluster coupling efficiency through adjustment of the laser and cluster parameters. Measurements of laser energy absorption in clusters have demonstrated that there exists an optimal laser pulse duration that depends on the average size of the clusters in the jet [7]. Furthermore, in experiments with a sequence of two laser pulses, kinetic energies of ions produced from cluster explosions have been shown to strongly depend on the relative delay between the two pulses [8]. Another experiment, measuring the ion kinetic energies, has indicated that the temporal profile of the laser pulse irradiating a cluster plays an important role in cluster heating. Differences up to a factor of 2 in ion energy have been achieved by varying the shape of the laser pulse [9].

Making use of optimal-control schemes in combination with laser pulse shaping can provide further insight into the problem of laser-cluster coupling optimization [10,11]. An optimal-control experiment on the production of highly charged ions resulting from the interaction of large xenon clusters ($N=10^4-10^6$ atoms per cluster) with an intense laser field has been recently performed in our group [12]. Adaptive pulse shaping under the control of a genetic algorithm (GA) [13] was used in the process of optimization. It was shown that the formation of highly charged ions dramatically increases by using a pulse shape consisting of a sequence of two pulses separated by a delay dependent on the average cluster size and the peak laser intensity. Another very recent optimal-control experiment on optimization of x-ray emission from argon clusters has also demonstrated the formation of a double-pulse structure as the optimal pulse shape [14]. These results indicate that there exists a specific time when the laser field is most efficiently coupled into the cluster.

Femtosecond laser-cluster interactions have been analyzed in terms of a number of models. For small clusters (up to 30 atoms/cluster) maximum energy absorption is governed by the mechanism of enhanced ionization, which occurs when the average distance between the atoms in the cluster reaches a critical value [15]. For medium-sized clusters ($\sim$1000–25 000 atoms per cluster), recently reported numerical simulations [16,17] reveal that the maximum energy gain is related to collective motion of the quasifree electrons in a cluster. Electron heating occurs due to dephasing of the motion of the electron cloud with respect to the driving laser field and is most efficient when the phase lag between them equals $\pi/2$. For large clusters several models have been introduced to analyze the cluster explosion. The nanoplasma model [5] for large clusters predicts an enhancement of the energy deposition into the cluster at a moment when the electron density becomes equal to 3 times the critical density. Under these conditions the plasma frequency in the cluster becomes equal to the frequency of the laser field, which leads to resonant plasma heating.

Therefore, each model predicts a single decisive moment during the laser-cluster interaction when the conditions for laser energy absorption are most favorable. As a result, the search for optimal laser energy deposition is usually limited to variation of a single time variable, which is either the laser pulse duration or the delay between a pair of pulses. While the optimal conditions found in this way provide insight into the laser-cluster interaction, the inherent restrictions in this approach stand in the way of acquiring a more complete physical picture. In the present paper we report optimal-control calculations of the interaction of xenon clusters with

*Current address: IRSAMC/LCAR, Université Paul Sabatier, 118 route de Narbonne, 31062 Toulouse Cedex 4, France.

intense shaped laser pulses where a GA controls 40 independent degrees of freedom in the laser pulse shape. The increased flexibility in the available pulse shapes in combination with the strength of evolutionary optimization leads to the determination of an optimum pulse shape for ionization of the cluster. To interpret the origin of the optimum pulse shape, calculations are also presented for the interaction of small to medium-size clusters ($N=108-5056$ atoms per cluster) with sequences of pulses with variable time delays and intensities. Our calculations show the influence of *several* mechanisms in the optimal cluster explosion and provide a qualitatively new understanding of the energy deposition for increasing cluster sizes.

II. MICROSCOPIC MODEL OF THE LASER-CLUSTER INTERACTION

The numerical simulations of the laser-cluster interactions were performed for small- to medium-size ($N=108-5056$ atoms per cluster) xenon clusters using a semiclassical molecular-dynamics approach [18]. The code used in the simulation initially assumes a cluster that consists of neutral xenon atoms that are arranged within a sphere on a bcc lattice with a lattice constant of 5 Å (providing a local density of the cluster equal to that of liquid xenon). In the absence of the laser field there are no interactions between the neutral cluster atoms. In the calculation bound electrons are not treated explicitly. Free electrons appear in the system as classical particles only after ionization of a parent atom takes place. Two ionization mechanisms are taken into account: field ionization and ionization by collisions of ions or atoms with fast electrons. In the former case the total electric field at the position of an atom is evaluated as the sum of the laser electric field and the field resulting from all charged particles in the cluster. The Ammosov-Delone-Krainov (ADK) formula [19] is used to calculate the rate of field ionization. Application of the ADK tunneling formula requires the total electric field at the ionizing atom to be sufficiently homogeneous over the distances relevant for tunneling and therefore imposes a minimum distance to the other charged particles. Consequently, the possibility of field ionization is disregarded if there is an electron within the proper volume of the atom, where the proper volume is defined as the effective volume occupied by one atom in a neutral cluster. Ionization by inelastic electron-ion collisions is only allowed to occur if the impacting electron passes through the proper volume of the atom. The collisional ionization rate is calculated as the product of the Lotz cross section [20] and the relative velocity of an impacting electron, divided by the proper volume of the atom. The product of the ionization rate and the time step duration gives the ionization probability within a small time interval. The trajectories of the ions and the ionized electrons are calculated from Newton's equations.

The efficiency of the laser-cluster coupling was evaluated by monitoring the number of "inner" or "outer" ionization events. Here "inner" ionization refers to the total number of quasifree electrons produced by field ionization or collisional ionization and "outer" ionization refers to the number of electrons that have been moved to a distance from the center of the cluster that corresponds to 20 times the cluster radius. At this distance the interaction of the ionized electron with the other particles can be ignored [21] and the electron is considered to be permanently removed from the cluster. The asymptotic properties of the outer ionized electrons (velocity and angular distribution) are evaluated taking into consideration the residual interaction of the electrons with the laser field from the time that they are removed from the calculation.

III. OPTIMAL-CONTROL CALCULATIONS

Optimization of the laser-cluster coupling efficiency was performed using adaptive laser pulse shaping controlled by a GA [10,13]. The clusters were exposed to shaped laser pulses that were derived by manipulation of the spectral phase function from a Fourier-transform-limited (FTL) laser pulse with a 25-fs full-width-at-half-maximum (FWHM) electric field envelope and a peak intensity of 0.01 a.u. (3.5×10^{14} W/cm^2). The spectral phase function was defined by 40 parameters distributed across the spectrum of the FTL pulse and spline interpolation at intermediate frequencies. The spectrum was centered at 800 nm, unless otherwise noted. Upon application of different phase functions a wide range of pulse shapes can be obtained.

The GA started with a random population of 30 individuals with each individual representing a specific spectral phase function and, consequently, a specific pulse shape. Each pulse shape was tested in our numerical model and assigned a fitness value, which was defined as the number of "inner" or "outer" ionization events. The fitness value was used as feedback for the GA in order to determine a new generation of 30 individuals. The genetic algorithm used in these calculations was the micro-GA available online [13]. We used elitism for one best individual, uniform crossover ($P_c=50\%$) and mutation ($P_m=2\%$) to create a new generation. GA optimizations, which were propagated for 200 generations, were performed for a cluster consisting of 108 Xe atoms. Thus, 6000 numerical experiments were performed in the course of the optimization, which took approximately 20 days on a 2.8-GHz Pentium processor. Due to the expense of calculating the Coulomb forces between every pair of charged particles, the computational time required for one numerical experiment is proportional to the square of the number of particles in the cluster. For this reason the optimizations were restricted to cluster sizes up to $N=108$.

The best pulse shapes that were found for the optimization of inner and outer ionization for Xe_{108} are shown in Fig. 1. Remarkably, the applied optimal phase patterns have broken the laser pulse up into a sequence of two pulses for inner ionization [Fig. 1(a)] and three pulses for outer ionization [Fig. 1(b)] with a separation of approximately 100 fs between the pulses. We note that in a subsequent run with a different set of random numbers controlling the crossover and mutation operators in the GA optimization procedure, optimized pulse shapes very similar to the ones shown in Fig. 1 were obtained. The sequence of random numbers involved in the code also influences the ionization dynamics. Whether or not ionization takes place is decided by compari-

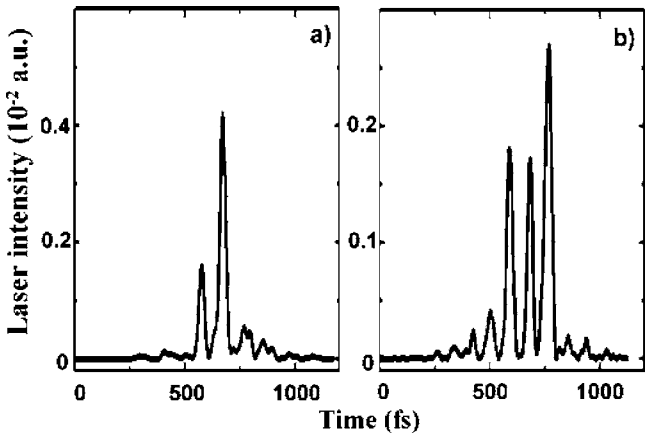

FIG. 1. Laser pulse shapes optimizing inner (a) and outer (b) ionization for a Xe_{108} cluster. The results were obtained using a genetic algorithm and show that inner and outer ionization are optimized by a sequence of two and three pulses, respectively.

son of the ionization probability with a random number. Therefore, similar to a real-life experiment, the outcome of our numerical experiment may vary if a calculation is repeated, even though the same pulse shape is applied. Finally, we note that we do not claim to have determined the global optimal pulse shapes for cluster ionization in our present optimal-control calculations. Rather we consider as the main result of the GA calculations the discovery of "interesting" pulse shapes that can help to reveal the dynamics of the laser-cluster interaction.

The pulse in Fig. 1(a) produces on average 430 electrons by field and collisional ionization, which compares favorably to 360 inner ionized electrons in the absence of the phase manipulation—i.e., using an FTL pulse with the same total energy. The pulse in Fig. 1(b) produces on average 280 outer ionization events, which is almost twice as much as an FTL pulse.

The difference between Figs. 1(a) and 1(b) points towards a qualitative difference between the optimal conditions for inner and outer ionization. In both cases the first pulse in the sequence is the trigger for the ionization process and the cluster expansion. The second pulse in Fig. 1(a) that optimizes inner ionization and that appears at the same delay in Fig. 1(b) suggests that there is a specific time during the interaction of a cluster with a laser pulse when inner ionization can be efficiently enhanced. The third pulse in Fig. 1(b) indicates that there are *two* instances when the conditions for outer ionization are favorably influenced.

To interpret the results of the optimal-control calculations, further simulations were performed using laser pulses consisting of a sequence of three FTL pulses. In a similar manner as in the optimal-control calculations inner and outer ionization of xenon clusters were monitored as a function of the time delays $\Delta\tau_1$ and $\Delta\tau_2$ between the first and second pairs of pulses in a three-pulse sequence. In doing so, we were interested in (a) confirming that a three-pulse sequence is indeed optimal for outer ionization of Xe_{108}, (b) determining whether a three-pulse sequence also represents an improvement over single pulses ($\Delta\tau_1=0$ and $\Delta\tau_2=0$) or two-pulse sequences ($\Delta\tau_1=0$ or $\Delta\tau_2=0$) for other cluster sizes, laser intensities, and laser wavelengths, and (c) being able to interpret the origin of the three-pulse optimum.

IV. CALCULATIONS WITH A SEQUENCE OF THREE PULSES

A. Cluster size effect

Simulations with a three-pulse sequence, where inner and outer ionization events of xenon clusters were monitored as a function of the time delays $\Delta\tau_1$ and $\Delta\tau_2$ between the first and second pairs of pulses, were performed for Xe_N clusters with $N=108-1524$. Each FTL laser pulse in the three-pulse sequence had a 25-fs FWHM electric field envelope and a peak intensity of 0.0033 a.u. (1.17×10^{14} W/cm^2). When both delays are zero the overlap of the three pulses results in a single 25-fs FTL pulse with a peak intensity of 0.01 a.u. (3.5×10^{14} W/cm^2)—i.e., the input pulse that was used, prior to modulation of the spectral phase, in the GA optimizations. Results for Xe_{108} and Xe_{302} are presented in Fig. 2, followed by results for Xe_{588} and Xe_{1524} in Fig. 3. A summary of the conditions that lead to maximum inner and outer ionization is shown in Tables I and II. A number of important observations can be made from Fig. 2. First of all, for both cluster sizes (Xe_{108} and Xe_{302} and for both inner and outer ionization, the best results are obtained when at least one of the delays is nonzero. A single FTL pulse ($\Delta\tau_1=\Delta\tau_2=0$) gives inferior results for both the inner and outer ionization. Second, the optimal pulse shape is qualitatively different depending on whether inner or outer ionization is monitored. Inner ionization in Xe_{108} [Fig. 2(a)] is maximized with a two-pulse sequence ($\Delta\tau_1=120$ fs, $\Delta\tau_2=0$), where the intensity of the second pulse is twice the intensity of the first pulse, in qualitative agreement with the GA optimization in Fig. 1(a). Optimization of outer ionization for Xe_{108} requires a laser pulse consisting alternatively of two or three peaks [Fig. 2(b)]. The latter result (see Table II) is qualitatively similar to the GA optimization in Fig. 1(b) and provides an equivalent fitness value. For slightly larger clusters (Xe_{302}) both inner and outer ionization are unambiguously optimized by a three-pulse sequence [Figs. 2(c) and 2(d)]. As shown in Fig. 3, this trend continues for increasing cluster sizes. A distinct maximum for the number of outer ionization events in Xe_{588} [Fig. 3(b)] is obtained by a sequence of three pulses with $\Delta\tau_1=225$ fs, $\Delta\tau_2=100$ fs. In the case of Xe_{1524} a search for the optimal delays $\Delta\tau_1$ and $\Delta\tau_2$ in a three-pulse sequence allowed us to identify the optimum at $\Delta\tau_1=400$ fs, $\Delta\tau_2=125$ fs [see Fig. 3(d)]. We note that the accuracy of determining the optimal pulse shape decreases with increasing cluster size due to the computational expense of the calculations for larger cluster sizes. For example, each point in Figs. 3(c) and 3(d) required approximately 10 h of computation, thus requiring about 50 days of computation on a 2.8-GHz Pentium-4 processor for the two plots shown. We also note that for larger cluster sizes the improvement that the three-pulse sequence represents over an FTL pulse dramatically increases. For example, for Xe_{1524} ionization by the optimal three-pulse sequence leads to 3538 outer ionized electrons, compared to 450 for an FTL pulse.

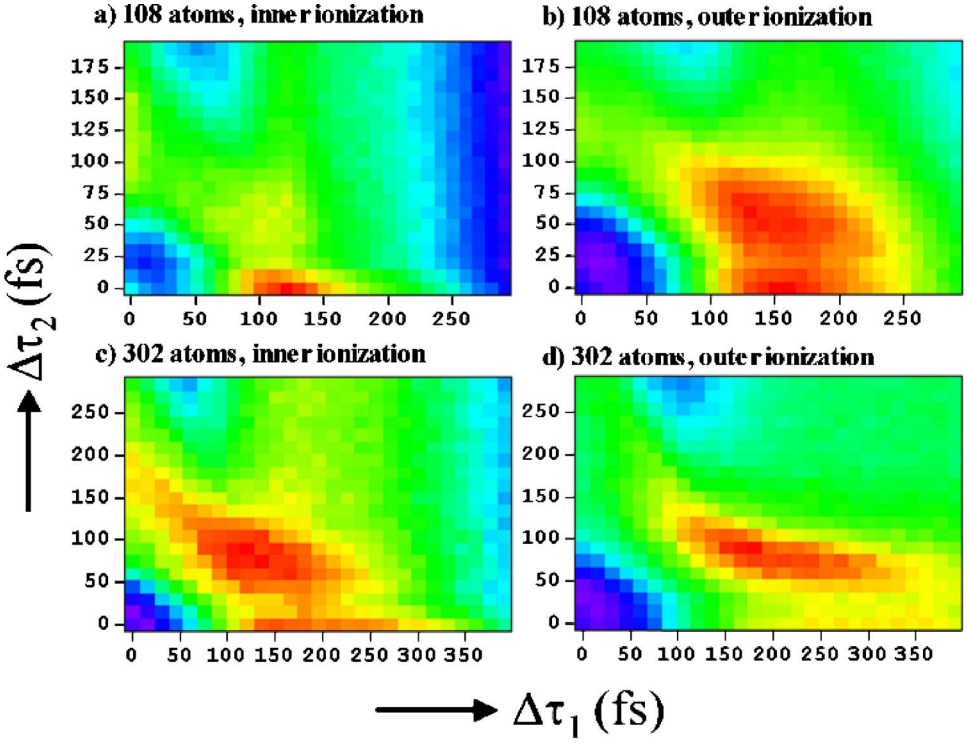

FIG. 2. (Color online). Contour plots showing the dependence of inner and outer ionization yields for Xe_{108} and Xe_{302} on the delays $\Delta\tau_1$ and $\Delta\tau_2$ in a three-pulse sequence consisting of 25-fs FTL pulses with a peak intensity of 0.0033 a.u. each. Red and blue colors (dark gray and black in grayscale version) signify maximum and minimum ionization levels, respectively: (a) inner ionization for Xe_{108} (max=445, min=340), (b) outer ionization for Xe_{108} (max=280, min=145), (c) inner ionization for Xe_{302} (max =1485, min=1090), and (d) outer ionization for Xe_{302} (max=745, min=255).

Our calculations clearly show an increase of the optimal delays for larger clusters (see Tables I and II). For Xe_{108} the optimal delays for outer ionization are found to be $\Delta\tau_1$ =140 fs and $\Delta\tau_2$=50 fs, which increase respectively to $\Delta\tau_1$ =400 fs and $\Delta\tau_2$=125 fs for Xe_{1524}. Though the range of cluster sizes accessed in our calculations differs from the cluster sizes that have been studied thus far experimentally, these observations are in line with trends found in earlier experimental observations [7,12].

B. Laser intensity effects

The evolution of the optimal pulse shapes with increasing laser intensity is shown in Fig. 4 for Xe_{108}, Xe_{302}, and Xe_{588} clusters. In these simulations the intensity of each pulse in the three-pulse sequence was 0.0066 a.u. (2.33×10^{14} W/cm^2), which is twice as much as in the previous calculations. Comparison of the results for Xe_{108} in Fig. 4 with the relevant results in Fig. 2 demonstrates the qualitative simi-

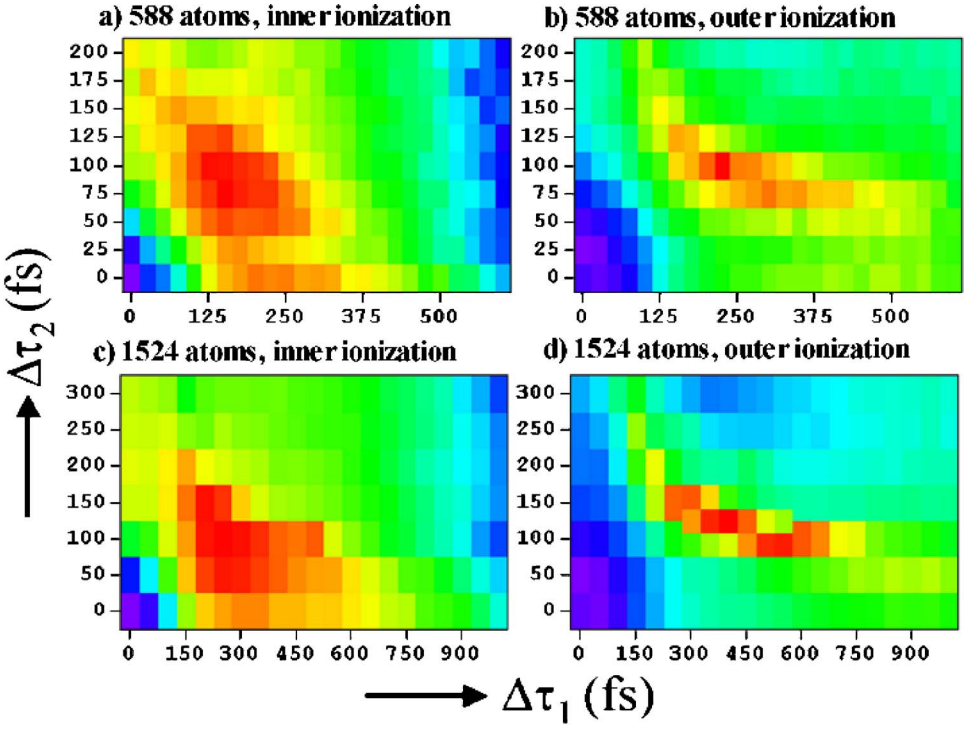

FIG. 3. (Color online). Contour plots showing the dependence of inner and outer ionization yields for Xe_{588} and Xe_{1524} on the delays $\Delta\tau_1$ and $\Delta\tau_2$ in a three-pulse sequence consisting of 25-fs FTL pulses with a peak intensity of 0.0033 a.u. each. Red and blue colors (dark gray and black in the gray scale version) signify maximum and minimum ionization levels, respectively: (a) inner ionization for Xe_{588} (max=3280, min=2250), (b) outer ionization for Xe_{588} (max=1455, min=330), (c) inner ionization for Xe_{1524} (max=9575, min=6290), and (d) outer ionization for Xe_{1524} (max =3540, min=450).

TABLE I. Summary of the conditions that lead to maximum inner ionization in a three-pulse sequence. The number of inner ionization events, the average internuclear distance $\langle r\rangle$, and the phase difference $\Delta\varphi$ between the collective electron oscillation and the oscillation of the laser field are given at the optimum time delays $\Delta\tau_1$ and $\Delta\tau_2$ that characterize the three-pulse sequence. Also shown in the table in brackets is the range of values of $\Delta\tau_1$ and $\Delta\tau_2$ where the number of inner ionized electrons remains above 90% of the difference between the maximum and the minimum ionization levels $[n > n_{\min}+0.9(n_{\max}-n_{\min})]$ as well as the corresponding values of the average internuclear distance $\langle r\rangle$ and the phase shift $\Delta\varphi$.

Cluster size N, laser intensity I (a.u.), laser wavelength λ (nm)	$\Delta\tau_1$ (fs)	$\Delta\tau_2$ (fs)	Inner ionization	$(\langle r\rangle/r_0)_{\Delta\tau_1}$	$\Delta\varphi_{\Delta\tau_1}/\pi$	$\Delta\varphi_{\Delta\tau_2}/\pi$
			(a) Cluster size dependence			
$N=108$, $I=0.0033$, $\lambda=800$	120 (100; 140)	0	445	1.4 (1.3; 1.5)	0.1 (0; 0.1)	0.1 (0; 0.1)
$N=302$, $I=0.0033$, $\lambda=800$	120 (75; 195)	90 (45; 120)	1483	1.2 (1.1; 1.6)	0.1 (0; 0.2)	0.54 (0.2; 0.8)
$N=588$, $I=0.0033$, $\lambda=800$	150 (100; 225)	100 (50; 125)	3278	1.3 (1.1; 1.53)	0.1 (0; 0.2)	0.54 (0.4; 0.7)
$N=1524$, $I=0.0033$, $\lambda=800$	250 (200; 500)	100 (50; 150)	9575	1.3 (1.2; 2)	0.1 (0; 0.4)	0.3 (0.2; 0.6)
			(b) Intensity dependence			
$N=108$, $I=0.0066$, $\lambda=800$	80 (70; 90)	0	509	1.3 (1.2; 1.4)	0.1 (0; 0.2)	0.1 (0; 0.2)
$N=302$, $I=0.0066$, $\lambda=800$	225 (105; 240)	0	1562	2.3 (1.4; 2.4)	0.45 (0; 0.5)	0.45 (0; 0.5)
	75 (60; 120)	90 (60; 120)	1572	1.2 (1.1; 1.47)	0	0.63 (0.2; 0.7)
$N=588$, $I=0.0066$, $\lambda=800$	125 (75; 175)	75 (50; 125)	3445	1.4 (1.1; 1.7)	0.1 (0; 0.2)	0.63 (0.3; 0.7)
			(c) Wavelength dependence			
$N=108$, $I=0.0033$, $\lambda=400$	50 (30; 60)	0	684	1.2 (1.1; 1.4)	0.2 (0.1; 0.4)	0.2 (0.1; 0.4)
$N=108$, $I=0.0033$, $\lambda=600$	90 (70; 100)	0	540	1.4 (1.3; 1.47)	0.2 (0; 0.3)	0.2 (0; 0.3)
$N=108$, $I=0.0033$, $\lambda=1064$	160 (140; 180)	0	373	1.4 (1.3; 1.5)	0.1 (0; 0.2)	0.1 (0; 0.2)

larity of the optimal pulse shapes obtained in both cases. The inner ionization is maximized with a two-pulse sequence [Fig. 4(a)], whereas outer ionization is optimized alternatively by a sequence of two or three pulses [Fig. 4(b)]. In this case the number of outer ionization events provided by the two-pulse sequence was around 10% higher than the one obtained with three pulses, whereas for lower intensity both sequences provided equivalent outer ionization. A new feature appears in the cases of Xe_{302} and Xe_{588} at the higher laser intensity—namely, the possibility to maximize outer ionization by just two laser pulses ($\Delta\tau_1=285$ fs, $\Delta\tau_2=0$ fs and $\Delta\tau_1=350$ fs, $\Delta\tau_2=0$ fs for Xe_{302} and Xe_{588}, respectively). Thus, unlike the lower-intensity case in Figs. 2(d) and 3(b) where outer ionization showed a clear maximum for a three-pulse sequence, the results in Figs. 4(d) and 4(f) display the possibility to obtain similar values for outer ionization using either two or three laser pulses.

A quantitative comparison of Figs. 2, 3, and 4 demonstrates a shortening of the optimal delays for both inner and outer ionization upon increase of the laser intensity (see Tables I and II). For example, the optimal delay between the two pulses for inner ionization in Xe_{108} decreases from 120 fs to 80 fs when the laser intensity is doubled, whereas for outer ionization in Xe_{108} the first delay in the optimal three-pulse sequence decreases, respectively, from $\Delta\tau_1=140$ fs to $\Delta\tau_1=100$ fs, while the second delay remains constant at $\Delta\tau_2=50$ fs. The shortening of the optimal delays upon increasing the laser intensity is in line with earlier experimental observations for large Xe clusters [7,12].

C. Laser wavelength effect

The dependence of the optimal pulse shapes for inner and outer ionization in Xe_{108} upon laser wavelength is shown in Fig. 5. We considered three additional wavelengths—namely, 400, 600, and 1064 nm. In all calculations the intensity of each pulse in the three-pulse sequence was again 0.0033 a.u. (1.17×10^{14} W/cm^2) and hence the results in Fig. 5 can be directly compared to the results for Xe_{108} in Fig. 2, where the

TABLE II. Summary of the conditions that lead to maximum outer ionization in a three-pulse sequence. The number of outer ionization events, the average internuclear distance $\langle r \rangle$, and the phase difference $\Delta\varphi$ between the collective electron oscillation and the oscillation of the laser field are given at the optimum time delays $\Delta\tau_1$ and $\Delta\tau_2$ that characterize the three-pulse sequence. Also shown in the table in brackets is the range of values of $\Delta\tau_1$ and $\Delta\tau_2$ where the number of outer ionized electrons remains above 90% of the difference between the maximum and the minimum ionization levels $[n > n_{\min} + 0.9(n_{\max} - n_{\min})]$ as well as the corresponding values of the average internuclear distance $\langle r \rangle$ and the phase shift $\Delta\varphi$.

Cluster size N, laser intensity I (a.u.), laser wavelength λ (nm)	$\Delta\tau_1$ (fs)	$\Delta\tau_2$ (fs)	Outer ionization	$(\langle r \rangle / r_0)_{\Delta\tau_1}$	$\Delta\varphi_{\Delta\tau_1}/\pi$	$\Delta\varphi_{\Delta\tau_2}/\pi$
			(a) Cluster size dependence			
$N=108$, $I=0.0033$, $\lambda=800$	150 (130; 200)	0	280	1.55 (1.45; 2)	0.1 (0.1; 0.6)	0.1 (0.1; 0.6)
	140 (110; 200)	50 (20; 80)	278	1.52 (0.3; 0.9)	0.2 (0; 0.6)	0.54 (0.2; 0.7)
$N=302$, $I=0.0033$, $\lambda=800$	165 (135; 285)	90 (60; 105)	740	1.46 (1.3; 2.1)	0.2 (0.1; 0.4)	0.7 (0.5; 0.7)
$N=588$, $I=0.0033$, $\lambda=800$	225 (200; 250)	100	1455	1.53 (1.46; 1.7)	0.2 (0.2; 0.3)	0.7 (0.7; 0.8)
$N=1524$, $I=0.0033$, $\lambda=800$	400 (250; 600)	125 (100; 150)	3538	1.7 (1.3; 2.4)	0.3 (0.1; 0.4)	0.6 (0.5; 0.7)
			(b) Intensity dependence			
$N=108$, $I=0.0066$, $\lambda=800$	110 (90; 140)	0	366	1.59 (1.4; 1.8)	0.2 (0.2; 0.3)	0.2 (0.2; 0.3)
	100 (90; 110)	50 (40; 60)	353	1.49 (1.4; 1.6)	0.2 (0.1; 0.2)	0.54 (0.4; 0.6)
$N=302$, $I=0.0066$, $\lambda=800$	285 (195; 330)	0	897	2.8 (2; 3.2)	0.54 (0.4; 0.6)	0.54 (0.4; 0.6)
	165 (105; 240)	75 (45; 90)	896	1.8 (1.4; 2.4)	0.3 (0; 0.5)	0.7 (0.45; 0.8)
$N=588$, $I=0.0066$, $\lambda=800$	350 (300; 425)	0	1601	3 (2.6; 3.5)	0.63 (0.45; 0.8)	0.6 (0.45; 0.8)
	200 (125; 350)	75 (50; 100)	1667	1.9 (1.4; 2.6)	0.3 (0.1; 0.6)	0.8 (0.6; 0.8)
			(c) Wavelength dependence			
$N=108$, $I=0.0033$, $\lambda=400$	70 (50; 70)	0	338	1.48 (1.2; 1.48)	0.6 (0.3; 0.6)	0.6 (0.3; 0.6)
$N=108$, $I=0.0033$, $\lambda=600$	110 (90; 130)	0	301	1.55 (1.4; 1.7)	0.2 (0.1; 0.4)	0.2 (0.1; 0.4)
	110 (90; 130)	30 (20; 40)	297	1.54 (1.4; 1.7)	0.3 (0.1; 0.5)	0.7 (0.5; 0.8)
$N=108$, $I=0.0033$, $\lambda=1064$	220 (140; 310)	80 (30; 130)	265	1.7 (1.3; 2.2)	0.2 (0; 0.4)	0.47 (0.2; 0.6)

spectrum was centered at wavelength of 800 nm. For all wavelengths considered, inner ionization of Xe_{108} is optimized by two pulses. The delay between the two pulses increases from 50 fs at 400 nm to 160 fs at a 1064 nm central wavelength [Figs. 5(a), 5(c), 2(a), and 5(e) and Table I]. The extension of the optimal delays with increasing wavelength is also observed for outer ionization [Figs. 5(b), 5(d), 2(b), and 5(f) and Table II]. These observations can be explained by the fact that the inner and outer ionization yields are higher for shorter wavelengths and hence cluster expansion occurs faster. For the shortest wavelength considered here (400 nm) only two laser pulses are required to optimize outer ionization, whereas for the longest wavelength considered here (1064 nm) the optimal pulse shape consists of three pulses. The calculations at 600 and 800 nm represent an intermediate case, exhibiting the transition of the optimal pulse shape from a two- to a three-pulse sequence.

V. ANALYSIS AND DISCUSSION

In order to interpret the pulse shapes that optimize inner and outer ionization and to reveal the mechanisms respon-

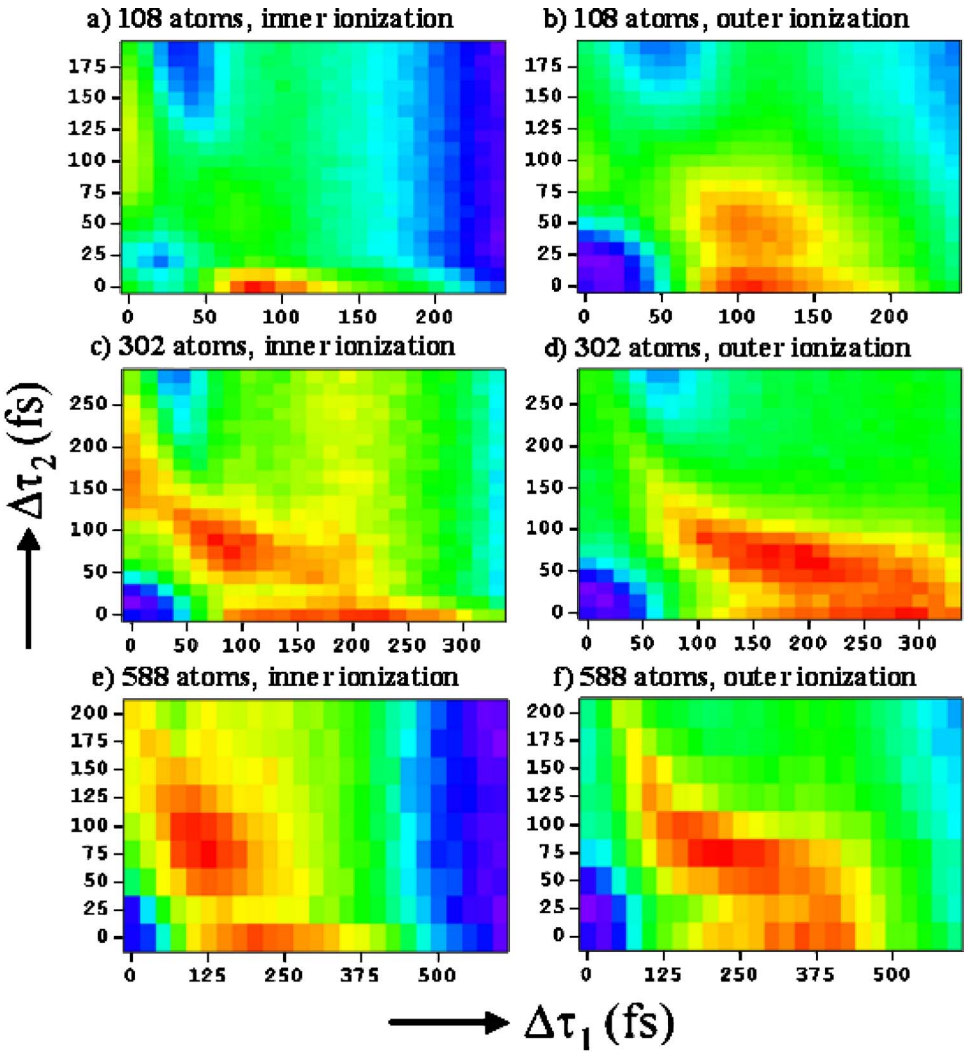

FIG. 4. (Color online). Contour plots showing the dependence of inner and outer ionization yields for Xe_{108}, Xe_{302}, and Xe_{588} on the delays $\Delta\tau_1$ and $\Delta\tau_2$ in a three-pulse sequence consisting of 25-fs FTL pulses with a peak intensity of 0.0066 a.u. each. Red and blue colors (dark gray and black in gray scale version) signify maximum and minimum ionization levels, respectively: (a) inner ionization for Xe_{108} (max=510, min=380), (b) outer ionization for Xe_{108} (max=370, min=210), (c) inner ionization for Xe_{302} (max=1575, min=1180), (d) outer ionization for Xe_{302} (max=900, min=385), (e) inner ionization for Xe_{588} (max=3445, min=2360), and (f) outer ionization for Xe_{588} (max=1670, min=535).

sible for this optimization, available numerical observables like the cluster expansion, the electron density, and the collective electron motion were monitored as a function of time and examined in relation to the models mentioned in the introduction.

The mechanism of enhanced ionization was previously observed in small molecules [22] and has been predicted in small clusters [15]. It suggests that ionization is favored when the internuclear separation between nearest-neighbor atoms in a cluster reaches a critical value during the cluster expansion. If the average distance between nearest-neighbor atoms in the cluster is defined as [15]

$$r(t) = \frac{1}{N}\sum_{\substack{i=1 \\ i\neq j}}^{N} \min\{|\vec{r}_i - \vec{r}_j|\}, \tag{1}$$

where $\vec{r}_i$ is the position of an ion and N the number of atoms in the cluster, then for small clusters the critical internuclear distance was empirically found in Ref. [15] to be approximately 1.5 times the equilibrium distance.

In the driven and damped harmonic oscillator model of Ref. [16] the cycle-averaged energy gain reaches a maximum when the eigenfrequency of the collective electron oscillation becomes equal to the laser frequency or, equivalently, when the phase shift $\Delta\varphi$ between the external driving field and the driven electron cloud becomes equal to $\pi/2$. In our case the electron oscillations randomize in the time interval between the pulses when no laser is present, but quickly reestablish themselves when the laser turns back on. This makes it possible to determine the phase delay of the collective electron oscillation with respect to the laser field during the second and—in particular—the third pulse in the sequence by means of a cross correlation of the instantaneous laser field and the oscillations of the center of mass of the quasifree electrons inside the cluster. Importantly, the phase shift depends on the delays that are applied between the laser pulses.

The nanoplasma model for large clusters considers the cluster as a small, spherical, and neutral plasma [5]. Early in the interaction, a shielding of the laser field occurs when the electron density rises. A field enhancement subsequently occurs when—as a result of outer ionization and cluster expansion—the electron density drops to 3 times the critical density. At this point the quasifree electrons are resonantly heated and a significant enhancement in the outer ionization is anticipated. The nanoplasma model is qualitatively similar to the model of collective electron oscillations [16]. Specifi-

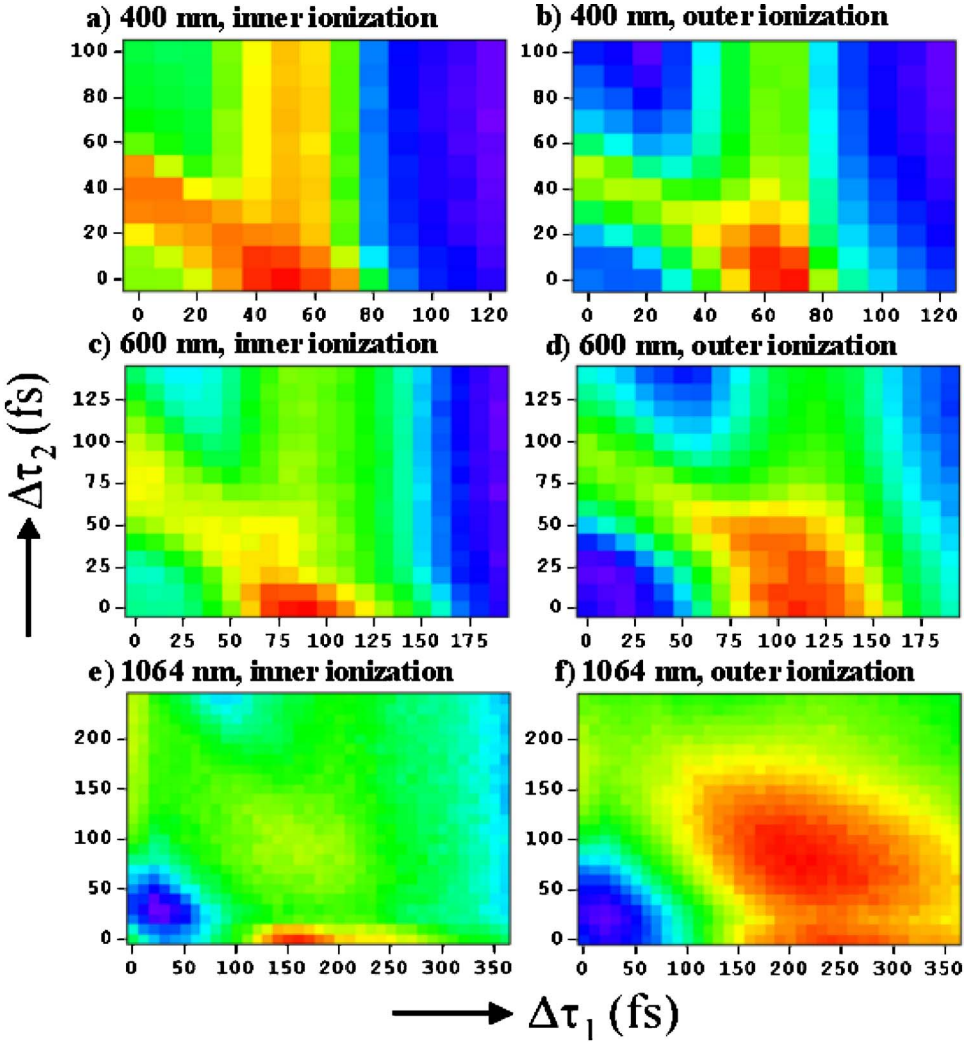

FIG. 5. (Color online). Contour plots showing the dependence of inner and outer ionization yields for Xe_{108} on the delays $\Delta\tau_1$ and $\Delta\tau_2$ in a three-pulse sequence consisting of 25-fs FTL pulses with a peak intensity of 0.0033 a.u. each for different wavelengths. Red and blue colors (dark gray and black in gray scale version) signify maximum and minimum ionization levels, respectively: (a) inner ionization for 400 nm (max=685, min=475), (b) outer ionization for 400 nm (max=340, min=160), (c) inner ionization for 600 nm (max=540, min=385), (d) outer ionization for 600 nm (max=305, min=160), (e) inner ionization for 1064 nm (max=375, min=290), and (f) outer ionization for 1064 nm (max=265, min=120).

cally, one can show that the predictions of the driven-and-damped oscillator model and the nanoplasma model become equivalent in the limit where the cluster stays charge-neutral (i.e., when outer ionization is negligible).

Analysis of our numerical results leads us to the conclusion that for all cluster sizes considered here, the enhancement of outer ionization with a three-pulse sequence can be explained by enhanced ionization [15] and resonant driving of the collective motion of the electrons [16]. The second pulse in the three-pulse sequence consistently occurs at a time when the optimal condition for enhanced ionization is satisfied, whereas the third pulse arrives when the collective motion of the quasifree electrons in the cluster resonantly couples with the laser field (see Table II). Accordingly, inspection of the calculations reveals an increase in the number of field ionization events at the optimal position of the second pulse and in the number of electron-impact ionization events during the third pulse.

Figure 6 presents details of the analysis of the optimal pulse for outer ionization of Xe_{302} [see Fig. 2(d)], where—as before—the laser intensity of each peak in the three-pulse sequence was 0.0033 a.u. (1.17×10^{14} W/cm^2). Ionization by the first pulse leads to expansion of the cluster under the influence of Coulomb forces. As shown in Fig. 6(b), the average internuclear distance becomes 1.5 times the equilibrium value at a delay of 170 fs after the maximum of the first pulse, which is almost exactly the value of $\Delta\tau_1$ in the optimum three-pulse sequence. At this point the collective electron oscillations are practically in phase with the laser field [$\Delta\varphi\cong0$, Fig. 6(c)] and play no role in the laser energy absorption. The value of the phase shift $\Delta\varphi$ between the collective electron oscillations and the laser field that occurs during the third pulse increases with the delay of that pulse and goes through $\pi/2$ for $\Delta\tau_2=70$ fs, close to the optimum time delay $\Delta\tau_2=90$ fs found in Fig. 2(d). A similar analysis applies to all cases where a three-pulse sequence is found to be the optimum for outer ionization. We note here that in the cases when the optimal values of $\Delta\tau_1$ and $\Delta\tau_2$ for inner or outer ionization cover a broad range of values [see, for example, Figs. 4(d) and 4(f)], assignment of the mechanisms responsible for the optimization can be only approximate.

In a number of cases it was observed that outer ionization could also be optimized by a sequence of just two laser pulses. In this case the mechanism that is operative during the second pulse depends on the cluster size, the laser intensity, and the laser wavelength. For Xe_{108} and a laser wavelength of 800 nm [Figs. 2(b) and 4(b)] the mechanism is enhanced ionization. In small clusters the electrons can gain

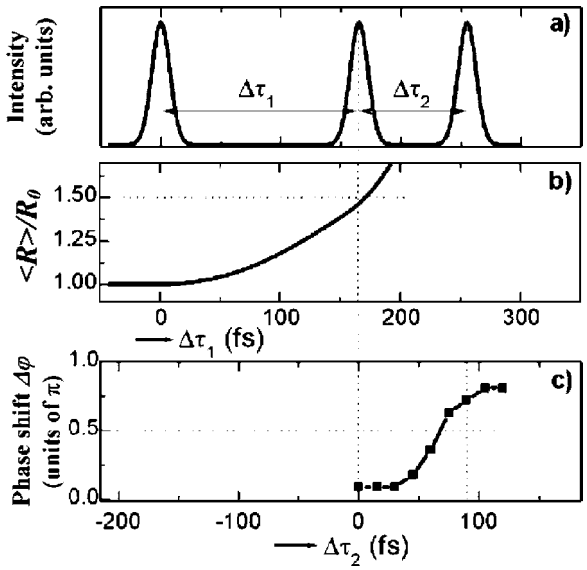

FIG. 6. Three-pulse sequence that maximizes outer ionization for Xe_{302} (a), along with the average internuclear distance between the atoms $\langle R\rangle/R_0$ as a function of $\Delta\tau_1$ (b) and the phase shift between the collective electron oscillation and the laser field oscillation during the third pulse as a function of $\Delta\tau_2$ (c). The occurrence of $\langle R\rangle/R_0=1.5$ and $\Delta\varphi=\pi/2$ at time delays close to $\Delta\tau_1$ and $\Delta\tau_2$ of the pulse in (a) supports the interpretation of the second and third pulses in the sequence in terms of enhanced ionization and resonant driving of the collective electron oscillation, respectively. We note that the phase shifts plotted in (c) were obtained in a series of calculations where $\Delta\tau_2$ was systematically varied and where $\Delta\varphi$ during the third pulse was determined for each value of $\Delta\tau_2$ using the procedure explained in the text.

enough energy to leave the cluster through enhanced ionization during the intense second pulse. This is especially true at higher laser intensities [Fig. 4(b)], when a two-pulse sequence gives more extensive outer ionization than a three-pulse sequence. By contrast, in larger clusters most quasifree electrons created by enhanced ionization cannot leave the cluster due to the higher space charge of the cluster and require further heating by the driving laser field, preferably at the collective electron oscillation resonance. This effect is illustrated by our calculations on Xe_{302} and Xe_{588}. At lower intensity [$I=0.0033$ a.u., Figs. 2(d) and 3(b)] a three-pulse sequence involving enhanced ionization and resonant excitation of the collective electron oscillation is clearly superior to a two-pulse sequence. However, for higher laser intensity [$I=0.0066$ a.u., Figs. 4(d) and 4(f)] it is possible to efficiently optimize outer ionization by just two pulses. Importantly though, the mechanism that is responsible for the efficient outer ionization is at that point the resonant collective motion of the quasifree electrons in the cluster (see Table II). Enhanced ionization on its own is not sufficient for maximizing outer ionization in larger clusters due to the high space charge in the cluster. Instead, the mechanism of resonant electron oscillations can efficiently heat and outer ionize electrons that were initially inner ionized by the first laser pulse, but remained trapped inside the cluster until the arrival of the second pulse. The two ionization mechanisms discussed also reveal themselves in the dependence of the optimal pulse shapes for outer ionization of Xe_{108} on laser wavelength [Figs. 2(b), 5(b), 5(d), and 5(f)]. For the longest wavelength (1064 nm) the outer ionization is optimized by a three-pulse sequence with involvement of both ionization mechanisms. For shorter wavelengths (800 and 600 nm) the optimal pulse consists alternatively of two or three peaks, associated, respectively, with the mechanism of enhanced ionization or in the case of three peaks with both mechanisms of ionization. The values of the optimal delays in the three-pulse sequence decrease from $\Delta\tau_1=220$ fs and $\Delta\tau_2=80$ fs for 1064 nm to $\Delta\tau_1=110$ fs and $\Delta\tau_2=30$ fs for 600 nm. The shift in $\Delta\tau_1$ is due to the higher ionization efficiency at shorter wavelengths, resulting in a faster cluster expansion. Furthermore, the reduction of $\Delta\tau_2$ with shorter wavelength is consistent with a resonant ionization mechanism, since for higher resonance frequency the resonance conditions are achieved earlier in time. For the shortest wavelength considered here (400 nm) optimization of outer ionization requires only two pulses. The optimal conditions for both ionization mechanisms are satisfied when the second pulse arrives at $\Delta\tau_1=70$ fs. In this case fast cluster expansion and electron heating during the intense second pulse effectively lead to shortening of $\Delta\tau_2$ to zero.

The results for inner ionization show trends qualitatively similar to outer ionization (Table I). In Xe_{108} inner ionization is maximized by a two-pulse sequence for any laser intensity and wavelength considered here [Figs. 2(a), 4(a), 5(a), 5(c), and 5(e)], while for larger clusters a third peak appears in the optimal pulse shapes [Figs. 2(c), 3(a), 3(c), 4(c), and 4(e)]. However, interpretation of the optimal pulse shapes for inner ionization turns out to be less transparent. Inspection of our calculations for Xe_{108} during the second pulse of an optimal two-pulse sequence shows that more than 70% of inner ionized electrons are produced by field ionization. This observation seems to be consistent with interpretation of the optimal pulse shape in terms of enhanced ionization, similar to the previously discussed case of outer ionization. Nevertheless, assigning the optimization of inner ionization to enhanced ionization is problematic. As shown in Table I, the second pulse in the optimal two-pulse sequence tends to arrive before the condition for enhanced ionization is fulfilled. Likewise, for larger clusters, where inner ionization is optimized by three pulses, the optimal delay for the second pulse does not exactly satisfy the conditions for the enhanced ionization mechanism.

An inner ionization event is recorded in our model when a quasifree electron is created inside the cluster. However, electrons with close to zero potential energy can stay quasibound to their parent atom. Since the interatomic barriers go up with increasing internuclear distance R, we would expect inner ionization to decrease with increasing R. On the other hand, the onset of outer ionization reduces shielding effects and facilitates inner ionization. The interplay between these two effects leads to the optimum for inner ionization at an internuclear distance that is intermediate between the equilibrium internuclear distance and the optimum for outer ionization.

We note that the arrival of the third pulse in the sequence that optimizes inner ionization (see Table I) matches the resonant coupling of the collective electron oscillations with

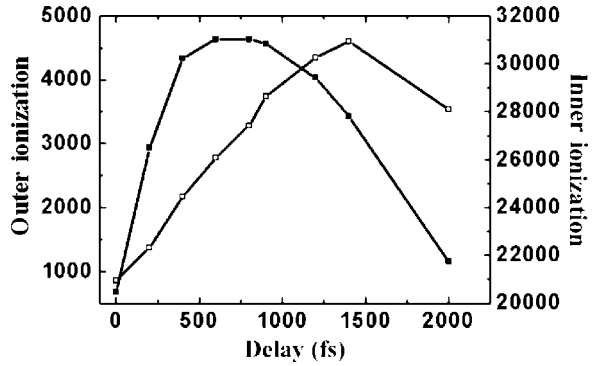

FIG. 7. Dependence of inner and outer ionization yields for Xe_{5056} on the delay in a two-pulse sequence consisting of 25-fs FTL pulses with a peak intensity of 0.005 a.u. each. Solid squares: the number of inner ionized electrons (right axis). Open squares: the number of outer ionized electrons (left axis).

the driving laser field (with the possible exception of Xe_{1524}, where as mentioned before, the optimal pulse shape was defined with 50 fs uncertainty). Accordingly, most electrons that are inner ionized during the third pulse are produced by electron-impact ionization.

VI. EXTRAPOLATION TO LARGER CLUSTERS ($N=5056$)

The calculations with sequences of three pulses discussed above are restricted to relatively small cluster sizes due to the computational expense involved in each calculation. In order to get insight into the evolution of ionization processes for larger clusters and to make our results relevant to experiments carried out with larger cluster sizes we performed a series of calculations with simple laser pulse shapes for Xe clusters containing 5056 atoms. These calculations and the predictions that they provide for several important and accessible experimental observables are described in this section.

A. Calculations with a sequence of FTL pulses

We first considered interaction of Xe_{5056} with a sequence of two FTL laser pulses with a 25-fs FWHM electric field envelope and a peak intensity of 0.005 a.u. (1.75×10^{14} W/cm^2). For a zero delay the overlap of the two pulses results in the previously used single FTL pulse with a 25-fs FWHM electric field envelope and a peak intensity of 0.01 a.u. (3.5×10^{14} W/cm^2). The efficiency of outer and inner ionization was examined as a function of the time delay between the two pulses. Results of these calculations are presented in Fig. 7, where the curves with solid and open symbols correspond to the number of inner and outer ionized electrons, respectively. For both inner and outer ionization a nonzero optimal delay between the two pulses is found. The number of inner ionization events obtained with an optimal delay of 600 fs between the two pulses is more than 30% higher than with a single FTL pulse with twice the peak intensity. Outer ionization is optimized with a 1400-fs delay between the two pulses and produces 5 times more outer ionized electrons than with a single FTL pulse with twice the peak intensity. Inspection of the calculations shows that this optimization of the outer ionization is accompanied by resonant coupling of the collective electron oscillations with the laser field during the second pulse in the sequence, when the phase shift between the electron collective oscillations inside the cluster and the laser field goes through $\pi/2$. We have seen no indication of enhanced ionization during the second pulse for both delays that optimize inner or outer ionization in agreement with the findings for two-pulse sequences reported for Xe_N ($N\geqslant302$) in Secs. IV and V.

Extrapolation of the results obtained in our calculations so far allows us to make a prediction for the values of the delays in a three-pulse sequence that would optimize outer ionization in Xe_{5056}. Applying a sequence of three FTL laser pulses with $\Delta\tau_1=1060$ fs and $\Delta\tau_2=150$ fs between the first and second pairs of pulses, where each pulse has a 25-fs FWHM electric field envelope and a peak intensity of 0.0033 a.u. (1.17×10^{14} W/cm^2), we obtained more than 11 500 outer ionization events. This is a considerable improvement over a single FTL pulse with 3 times higher peak intensity, which leads to 860 outer ionization events and compares favorably to 4600 outer ionized electrons obtained in the previous optimal case of two pulses (Fig. 7). We note that this significant enhancement of the outer ionization yield was achieved even though our prediction for the optimal values of delays $\Delta\tau_1$ and $\Delta\tau_2$ does not provide exact matching of the second and third peaks in the sequence to the optimal conditions for the two mechanisms of ionization. Thus, further improvement of outer ionization efficiency may be possible with more accurate estimates of the optimal delays in a three-pulse sequence.

B. Electron energy and angular distributions

In order to explore the relation between the optimal conditions for inner or outer ionization and the optimal conditions for energy coupling from the laser field into the cluster, the electron kinetic energy and angular distribution at the end of the laser-cluster interaction were examined. This also gives us a possibility to qualitatively compare the results of our simulations to earlier experimental measurements [3,4,23], where the occurrence of features in the electron kinetic energy distributions due to resonant heating of the clusters has been discussed.

Figure 8(a) shows asymptotic electron kinetic energy distributions of outer ionized electrons from Xe_{5056} for four different laser pulse shapes—namely, a single FTL pulse with a 25-fs FWHM electric field envelope and a peak intensity of 0.01 a.u. (3.5×10^{14} W/cm^2) (solid squares), two sequences of two FTL pulses with a 25-fs FWHM electric field envelope and a peak intensity of 0.005 a.u. (1.75×10^{14} W/cm^2) with a delay of 600 fs (open squares) and 1400 fs (solid triangles) between them, respectively, and finally a sequence of three FTL pulses with a 25-fs FWHM electric field envelope and a peak intensity of 0.0033 a.u. (1.17×10^{14} W/cm^2) with delays $\Delta\tau_1=1060$ fs and $\Delta\tau_2=150$ fs between the first and second pairs of pulses (open triangles).

All electron kinetic energy distributions are qualitatively similar and display a single-peaked structure. Furthermore, an increase in the yield of outer ionization through the appli-

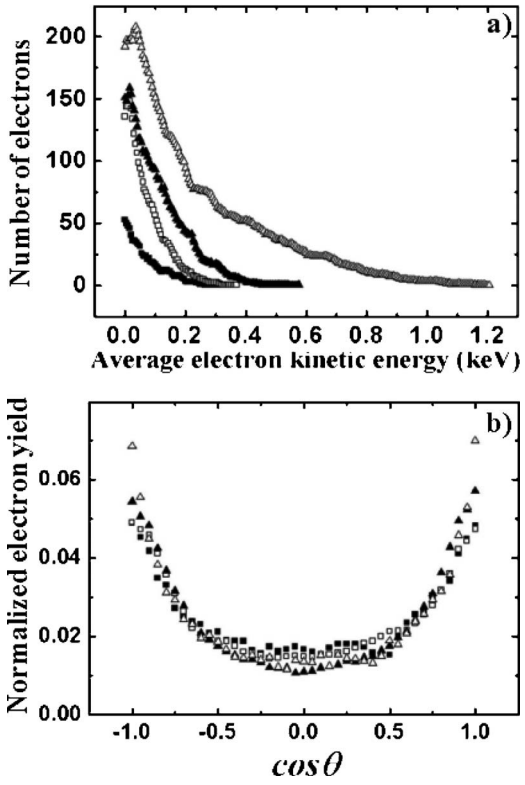

FIG. 8. (a) Asymptotic electron kinetic energy distributions and (b) electron angular distributions of outer ionized electrons from Xe_{5056} for four different laser pulse shapes—namely, a single 25-fs FTL pulse with a peak intensity of 0.01 a.u. (solid squares), a sequence of two 25-fs FTL pulses with a peak intensity of 0.005 a.u. each with a delay of 600 fs (open squares) and 1400 fs (solid triangles), and a sequence of three 25-fs FTL pulses with a peak intensity of 0.0033 a.u. each with delays $\Delta\tau_1=1060$ fs and $\Delta\tau_2=150$ fs (open triangles).

cation of a better laser pulse shape is accompanied by an enhancement of the average kinetic energy of outer ionized electrons. For a single FTL pulse the average temperature of the electrons leaving the cluster is approximately 85 eV. Electrons that are ejected from the cluster after the first pulse in a two-pulse sequence are characterized by an electron temperature of about 80 eV. The average temperature of the electrons that are emitted after the second laser peak depends on the value of delay between the laser peaks and grows from 90 eV for a delay of 600 fs to a maximum of 140 eV with a delay of 1400 fs between the two pulses. The average electron temperature goes down when the delay is further increased. So the 1400 fs delay that optimizes the number of outer ionized electrons (see Fig. 7) also provides the most efficient laser energy transfer to the electrons emitted from a Xe_{5056} cluster.

The sequence of three pulses with delays $\Delta\tau_1=1060$ fs and $\Delta\tau_2=150$ fs between the first and second pairs of pulses provides electrons that are characterized by an average electron temperature of 270 eV, which compares favorably to the optimal two-pulse sequence. We note also that for any considered laser pulse shape the single-peaked structure of electron kinetic energy distributions remains unaffected. Qualitatively similar results were observed experimentally in [4] for slightly larger clusters.

Asymptotic electron angular distributions are given in Fig. 8(b). The distributions are normalized to the number of electrons emitted from the cluster and are shown for the same conditions as in Fig. 8(a). For all pulse shapes quantitatively similar electron angular distributions are observed with the majority of electrons being ejected along the laser polarization axis. We have also observed that electrons that leave the cluster after the first peak in a two-pulse sequence have angular distributions equivalent to the ones acquired after the second laser peak. Our observation that the electron angular distribution is peaked along the laser polarization axis is consistent with earlier experimental results for larger Xe clusters [4].

VII. CONCLUSION

In conclusion, we have presented numerical simulations of cluster ionization by intense shaped laser pulses. We have shown that the interaction of Xe_N ($N=108-1524$) clusters with an intense laser pulse is governed by two special instants of time when the conditions for laser energy absorption in the cluster are most favorable. The mechanisms that are operative at these moments are enhanced ionization and resonant driving of collective electron oscillations, the former having its origin in intense field interactions of small molecules and the latter in plasma physics. Our results thus show how the physics of clusters in intense laser fields evolves from the dynamics of small molecules and provide insight into the onset of collective effects when increasingly large clusters are studied.

Our simulations predict that for selected combinations of cluster size, laser intensity, and laser wavelength the ionization may be optimized by a three-pulse sequence involving both enhanced ionization and resonant driving of the collective electron oscillations. We have observed that altering the conditions of the laser-cluster interaction (for example, an increase of the laser intensity) can simplify the dynamics, so that only one mechanism remains involved. This may be the reason why two earlier optimal-control experiments [12,14] observed a two-pulse sequence as the optimal pulse shape for the production of highly charged ions and x-ray photons: both experiments were performed with larger clusters and at higher intensities, and moreover made use of samples containing a broad cluster size distribution. Quantitative verification of our results requires an experiment on size-selected clusters, where the efficiency of laser energy coupling into a cluster of a given size can be measured as a function of applied pulse shapes and the mechanisms of laser-cluster energy transfer can be determined experimentally.

ACKNOWLEDGMENTS

This work is part of the research program of the "Stichting voor Fundamenteel Onderzoek der Materie" (FOM), which is financially supported by the "Nederlandse organisatie voor Wetenschappelijk Onderzoek" (NWO). The research of S.Z. was supported by the EU Marie Curie program. Ch.S. acknowledges EU Marie Curie Research Training Network MRTN-CT-2003-505138 (XTRA).

[1] T. Ditmire, R. A. Smith, J. W. G. Tisch, and M. H. R. Hutchinson, Phys. Rev. Lett. **78**, 3121 (1997).
[2] T. Ditmire, J. W. G. Tisch, E. Springate, M. B. Mason, N. Hay, R. A. Smith, J. Marangos, and M. H. R. Hutchinson, Nature (London) **386**, 54 (1997).
[3] Y. L. Shao, T. Ditmire, J. W. G. Tisch, E. Springate, J. P. Marangos, and M. H. R. Hutchinson, Phys. Rev. Lett. **77**, 3343 (1996).
[4] E. Springate, S. A. Aseyev, S. Zamith, and M. J. J. Vrakking, Phys. Rev. A **68**, 053201 (2003).
[5] T. Ditmire, T. Donnelly, A. M. Rubenchik, R. W. Falcone, and M. D. Perry, Phys. Rev. A **53**, 3379 (1996).
[6] D. Attwood, *Soft X-rays and Extreme Ultraviolet Radiation* (Cambridge University Press, Cambridge, England, 1999).
[7] J. Zweiback, T. Ditmire, and M. D. Perry, Phys. Rev. A **59**, R3166 (1999).
[8] E. Springate, N. Hay, J. W. G. Tisch, M. B. Mason, T. Ditmire, J. P. Marangos, and M. H. R. Hutchinson, Phys. Rev. A **61**, 044101 (2000).
[9] K. J. Mendham, J. W. G. Tisch, M. B. Mason, N. Hay, and J. P. Marangos, Opt. Express **11**, 1357 (2003).
[10] R. S. Judson and H. Rabitz, Phys. Rev. Lett. **68**, 1500 (1992).
[11] A. M. Weiner, Rev. Sci. Instrum. **71**, 1929 (2000).
[12] S. Zamith, T. Martchenko, Y. Ni, S. A. Aseyev, H. G. Muller, and M. J. J. Vrakking, Phys. Rev. A **70**, 011201 (2004).
[13] D. L. Carroll at http://cuaerospace.com/carroll/ga.html
[14] A. S. Moore, K. J. Mendham, D. R. Symes, J. S. Robinson, E. Springate, M. B. Mason, R. A. Smith, J. W. G. Tisch, and J. P. Marangos, Appl. Phys. B: Lasers Opt. **80**, 101 (2005).
[15] C. Siedschlag and J. M. Rost, Phys. Rev. Lett. **89**, 173401 (2002).
[16] U. Saalmann and J. M. Rost, Phys. Rev. Lett. **91**, 223401 (2003).
[17] C. Jungreuthmayer, M. Geissler, J. Zanghellini, and T. Brabec, Phys. Rev. Lett. **92**, 133401 (2004).
[18] E. S. Toma and H. G. Muller, Phys. Rev. A **66**, 013204 (2002).
[19] M. V. Ammosov, N. B. Delone, and V. P. Krainov, Zh. Eksp. Teor. Fiz. **91**, 2008 (1986).
[20] W. Lotz, Z. Phys. **216**, 241 (1968).
[21] I. Last and J. Jortner, Phys. Rev. A **62**, 013201 (2000).
[22] T. Seideman, M. Yu. Ivanov, and P. Corkum, Phys. Rev. Lett. **75**, 2819 (1995).
[23] V. Kumarappan, M. Krishnamurthy, and D. Mathur, Phys. Rev. A **66**, 033203 (2002).